

	001
	002
	003
	004
	005
	006
The Importance of Initial Conditions in Seasonal	007
Predictions of Antarctic Sea Ice	008
	009
Elio Campitelli ^{1,2*} , Ariaan Purich ^{1,2} , Julie Arblaster ^{1,2} ,	010
Eun-Pa Lim ³ , Matthew C. Wheeler ³ , Phillip Reid ³	011
	012
	013
¹ School of Earth, Atmosphere and Environment, Monash University, Kulin	014
Nations, Clayton, Victoria, Australia..	015
	016
² SARC Special Research Initiative for Securing Antarctica's	017
Environmental Future, Clayton, Kulin Nations, Victoria, Australia.	018
	019
³ Research, Bureau of Meteorology, Melbourne, Australia.	020
	021
	022
*Corresponding author(s). E-mail(s): elio.campitelli@monash.edu ;	023
	024
	025
	026
	027
	028
	029
	030
	031
	032
	033
	034
	035
	036
	037
	038
	039
	040
	041
	042
	043
	044
	045
	046

Abstract

Accurate Antarctic sea-ice forecasts are crucial for climate monitoring and operational planning, yet they remain challenging due to model biases and complex ice-ocean-atmosphere interactions. The two versions of the Australian Bureau of Meteorology's ACCESS seasonal forecast system, ACCESS-S1 and ACCESS-S2, use identical model configuration and differ only in their initial conditions; primarily in that ACCESS-S2 does not assimilate sea-ice observations, whereas ACCESS-S1 does.

This provides a convenient opportunistic experiment to assess the role of initial conditions on Antarctic sea-ice forecasts using more than 20 years of fully coupled simulations with two 9-member ensembles. Our analysis reveals that both systems experience an extended melt season and delayed growth phase compared with observations. This leads to a significant negative sea-ice extent bias, which is corrected only in ACCESS-S1 by the data assimilation system. The impact of the differing initial conditions on forecast errors varies dramatically by season: summer and autumn initial conditions (January-April) provide predictive skill for up to three months, with February initial conditions being particularly crucial.

047 In contrast, winter forecasts of the two systems are statistically indistinguishable
048 after only two weeks. Regional analysis of forecast skill suggests that this
049 winter predictability barrier is most dramatic over East Antarctica, where even
050 ACCESS-S1 shows negative skill. These findings highlight the critical importance
051 of comprehensive year-round sampling in predictability studies and suggest that
052 operational sea-ice data assimilation efforts should prioritize the summer-autumn
053 period when initial conditions have maximum impact on forecast skill.

054
055 **Keywords:** sea ice, seasonal predictability, initial conditions, forecasting

056
057
058
059

060 **Introduction**

061

062 Accurately modelling Antarctic sea ice is essential for understanding processes and
063 improving climate projections to inform adaptation strategies. Accurate seasonal to
064 sub-seasonal forecasts are also crucial for operation contingency planning in and
065 around the Antarctic continent, including scientific missions, fisheries, and tourism^{1;2}.
066

067 Improvements in modelled sea-ice might also help improve weather forecasts over and
068 away from sea-ice regions^{3–5}.

069

070 However, progress in Antarctic sea-ice forecasting system has lagged behind Arctic
071 sea-ice forecasts due to model biases, and inherent large variability and complexity^{6;7}.
072

073 Dynamical seasonal forecasts of summer Antarctic sea ice have been shown to perform
074 worse than relatively simpler statistical methods⁸ and machine learning approaches (e.g.
075 Dong et al.⁹, Lin et al.¹⁰), which also underscores the need for better understanding
076 and physical modelling of sea-ice dynamics, and drivers of its variability.

077

078 Good initial conditions are generally required for a good forecast, however, it is not
079 entirely known to what extent accurate sea-ice initial conditions affect the quality of
080 the forecast and at what timescales. Exploring seasonal predictions of Arctic sea ice,
081 Guemas et al.¹¹ found that sea-ice initial conditions are important in autumn to predict
082 summer sea ice, but the impact wasn't as dramatic when predicting winter sea ice. Day
083

084

et al.¹² also found seasonally-varying differences in the effect of initialisation, noting that accurate Arctic sea-ice thickness leads to improved sea-ice forecasts initialised in July but not when initialised in January.

For the Antarctic, Holland et al.¹³ studied the initial-value predictability of Antarctic sea ice in a perfect model study using the CCSM3 model. They found that sea-ice and ocean initial conditions provide predictive information to forecast sea-ice edge location several months in advance and that some predictability is retained for up to two years thanks to ocean heat content anomalies that are advected eastward. This is in contrast with Marchi et al.¹⁴, who ran perfect model experiments to argue that uncertainty in the predicted atmospheric state and evolution is the main driver of uncertainty in Antarctic sea-ice extent prediction on seasonal timescales, with sea-ice and ocean initial conditions having lesser importance. More recently, Morioka et al.¹⁵ studied decadal forecasts of Antarctic sea ice and found that initialising ocean and sea ice improved the correlation between simulated and observed sea-ice concentration evolution in the Amundsen–Bellingshausen Sea. It is hard to compare these studies since they are based on forecasts initialised at different times of the year and different frameworks: Holland et al.¹³ ran 20 ensemble members initialised on the 1st of January of a particular year, Marchi et al.¹⁴ ran forecasts from the 1st of March and 1st of September, and Morioka et al.¹⁵ ran forecasts only from the 1st of March. Marchi et al.¹⁴ also used a coupled ocean–sea-ice model instead of a fully coupled model like Holland et al.¹³ did. Morioka et al.¹⁵ used observed sea-ice initial conditions and compared with observations, while Marchi et al.¹⁴ and Holland et al.¹³ were perfect model studies.

In October 2021 the Australian Bureau of Meteorology (BoM) upgraded the Australian Community Climate and Earth System Simulator – Seasonal (ACCESS-S) from version S1 to S2. While the base model remained the same, the change in version was focused on using ocean, sea-ice and land initial conditions generated by the BoM instead of depending on the UK Met Office. Crucially, compared to ACCESS-S1, ACCESS-S2

139 does not assimilate sea-ice observations, so sea ice is only affected by the ocean and
140 atmospheric data assimilation via the coupled integration.
141

142 Since model configuration is identical between ACCESS-S1 and ACCESS-S2, they
143 form a sort of “opportunistic experiment” where the same forecasting model was run
144 over a long period of time with multiple ensemble forecasts initialised throughout the
145 year, with the only difference being the initial conditions. This provides an opportunity
146 to test the effect of sea-ice initial conditions on the forecast of sea-ice concentrations
147 and the climate.
148

149 In this study we compare sea-ice hindcasts produced by ACCESS-S1 and ACCESS-S2.
150 We focus on seasonality of errors and biases and the effect of the data assimilation
151 system. This comparison will inform future work with the prediction system as a
152 research tool to better understand the dynamics and variability of the Antarctic sea
153 ice and its impacts on the climate system as well as to explore the potential of using
154 its sea-ice forecasts for decision-making. The work will also serve as a benchmark for
155 future prediction systems to attempt to improve upon.
156

166 **Data and methods**

167 **ACCESS-S2**

168 ACCESS-S2¹⁶ is the Bureau of Meteorology’s seasonal forecast system which became
169 operational in October 2021, replacing the ACCESS-S1 system¹⁷. The model com-
170 ponents of both ACCESS-S2 and ACCESS-S1 are identical with the same numbers
171 of levels and resolution. They consist of the Global Atmosphere 6.0 (GA6)^{18;19}, the
172 Unified Model’s Global Land 6.0^{19;20}, NEMO Global Ocean 5.0^{21;22} and Global Sea
173 Ice 6.0 [CICE; Rae et al. ²³]. The atmosphere has a N216 horizontal resolution (~60 km
174 in the mid-latitudes) with 85 vertical levels. The land model uses the same horizontal
175

grid as the atmosphere with four soil levels. The ocean component has a nominal	185
horizontal resolution of $1/4^\circ$ with 75 vertical levels. The sea-ice component, based on	186
CICE version 4.1, has the same resolution as the ocean component and five sea-ice	187
thickness categories as well as an open water category.	188
	189
	190
	191
Both systems take atmospheric initial conditions derived from ERA-interim ²⁴ for	192
their hindcasts. The main difference between the hindcasts of the two systems are the	193
ocean and sea-ice initial conditions. ACCESS-S1's ocean and sea-ice initial conditions	194
come from the Met Office FOAM system, which uses a multivariate, incremental	195
three-dimensional variational (3D-Var), first-guess-at-appropriate-time (FGAT) data	196
assimilation scheme ²⁵ and assimilates sea surface temperature (SST), sea surface height	197
(SSH), in situ temperature and salinity profiles, and satellite observations of sea-ice	198
concentration using the EUMETSAT OSISAF product described in the next section.	199
ACCESS-S2, on the other hand, is initialised from ocean conditions generated by the	200
BoM weakly coupled ensemble data assimilation scheme described in Wedd et al. ¹⁶ .	201
This scheme uses an optimal interpolation method and assimilates temperature and	202
salinity profiles from EN4 ²⁶ . SSTs are nudged to Reynolds OISSTv2.1 ²⁷ in areas where	203
SSTs are over 0°C and Sea Surface Salinity is weakly nudged to the World Ocean Atlas	204
2013 climatology ²⁸ .	205
	206
	207
	208
	209
	210
	211
	212
	213
	214
	215
Of most relevance for this work, sea-ice concentrations are not assimilated in ACCESS-	216
S2. Assimilation cycles are performed daily. The coupled model runs for 24 hours	217
initialised from the previous cycle. Then the restart file fields of the ocean component	218
are used as first guess in the data assimilation cycle and the innovations are used to	219
build the next ocean initial conditions for the following cycle. The atmosphere fields	220
from that daily integration are not used and instead the model atmosphere is initialised	221
using ERA-Interim. The sea-ice initial conditions for the next cycle are the unaltered	222
output of the previous daily integration. Then the cycle starts again and the coupled	223
model runs for another 24 hours. During this integration the sea-ice component is	224
	225
	226
	227
	228
	229
	230

231 affected by the ocean innovations and the new atmosphere initial conditions via the
232 coupler.

234
235 The ACCESS-S1 hindcast set is made up of nine members created by perturbing the
236 atmospheric fields only with a random field perturbation¹⁷ and runs for 217 days for
237 the period 1990–2012 initialised at the first of every month. The ACCESS-S2 hindcast
238 set used in this study runs for the period 1981–2018. Ensemble members are created in
239 the same manner as ACCESS-S1 members, however, due to computing cost limitations,
240 only three members per forecast initialisation date were run for 279 days. Bigger
241 ensembles were generated by aggregating several three-member ensembles initialised
242 on successive days¹⁶. Here, we build a nine-member time-lagged ensemble from three
243 consecutive three-member forecasts initialised at the first of every month and the two
244 previous days and run for 279 days. We analyse the ensemble mean hindcasts unless
245 otherwise specified.

246
247 Anomalies for each hindcast set are taken with respect to their own climatology specific
248 to each initialisation date and forecast lead time, for the period 1990–2012. This serves
249 as a first-order correction of model bias and drift. For monthly means, we define “0
250 lead time months” as the monthly mean forecast of the same month of initialisation.
251
252 Besides sea-ice concentration, we also analyse mean sea-ice thickness, which we compute
253 as total sea-ice volume divided by total sea-ice area.

254

255

256 **Verification datasets**

257

258 For verification we use satellite-derived sea-ice concentration, which estimates the
259 proportion of each grid area that is covered with ice. Datasets derived using different
260 algorithms and satellite platforms, each have their own biases and uncertainties.
261 Estimates of inter-product uncertainty of sea-ice extent (SIE, defined here as the total
262 region of the Southern Ocean with at least 15% sea-ice cover) are of the order of 0.5
263
264

million km^2 ²⁹. As will be shown below, this spread is minimal compared with the typical errors in the ACCESS-S2 and ACCESS-S1 forecasts, so the overall conclusions of this study are independent of the verification dataset used.

We use NOAA/NSIDC's Climate Data Record V4 [CDR; Meier et al.³⁰] as the primary sea-ice verification dataset. It takes the maximum value of the NASA Team³¹ and NASA Bootstrap³² sea-ice concentration products to reduce their low concentration bias^{30;33}. Both source algorithms use data from the Scanning Multichannel Microwave Radiometer (SMMR) on the Nimbus-7 satellite and from the Special Sensor Microwave/Imager (SSM/I) sensors on the Defense Meteorological Satellite Program's (DMSP) -F8, -F11, and -F13 satellites. The data have a spatial resolution of 25 by 25 km and daily from November 1978 onwards.

The European Organisation for the Exploitation of Meteorological Satellites (EUMETSAT) Ocean and Sea Ice Satellite Application Facility [OSI; EUMETSAT Ocean and Sea Ice Satellite Application Facility³⁴] based on the SSMIS sensor is another satellite-derived sea-ice concentration product. It is based on mostly the same sensors as the NOAA CDR but computed independently using different algorithms. Figures prepared with this dataset are provided in the supplementary material and do not differ significantly from the ones prepared using CDR.

Error measures

For evaluation purposes, we use a series of measures. Sea-ice extent is defined as the area of the ocean at least 15% covered by sea-ice. This threshold is motivated by the limitations in satellite retrieval, which is increasingly unreliable for lower sea-ice concentrations³⁵.

Pan-Antarctic (net) sea-ice extent serves as a hemispheric measure of the amount of sea ice, but it does not take into account the spatial distribution. A model could have

323 a relatively accurate extent of the net ice but with different regional distributions. To
324 account for location errors, we computed the Root Mean Squared Error (RMSE) of
325 grid-point sea-ice concentration anomalies.
326

327 We compute RMSE as the square root of the area-averaged squared differences between
328 grid-point forecasted and observed sea-ice concentration anomalies. We compute a
329 pan-Antarctic RMSE by averaging over the whole NOAA/NSIDC CDRV4 Southern
330 Hemisphere domain, and also a zonally-varying RMSE computed over 15 longitude
331 slices 24° wide around Antarctica.
332

333 All error measures were computed on the NOAA/NSIDC CDRV4 domain grid, to
334 which model output was bilinearly interpolated. Note that the ACCESS CICE model
335 grid has resolution between two and three times higher than NOAA/NSIDC CDRV4.
336

337 Forecast errors are also compared with hypothetical forecasts based on the persistence
338 of anomalies and on climatology. The persistence forecast is generated by extending
339 the observed sea-ice concentration anomalies the day of the forecast initialisation and
340 comparing it with the actual anomalies observed. The climatological forecast error is
341 computed as the standard deviation of daily anomalies.
342

343 As a measure of forecast improvement over the hypothetical forecast, we use the skill
344 score³⁶, defined as
345

346

347
$$S = 1 - \frac{RMSE_f}{RMSE_r}$$

348

349 Where $RMSE_f$ is the RMSE of the forecast, $RMSE_r$ is the RMSE of the reference
350 forecast. Negative skill score indicates that the forecast is worse than the reference
351 forecast while positive values indicate an improvement. A perfect forecast would have
352 zero RMSE and thus a skill score of 1.
353

354

355

356

Computational procedures

369
370

We performed all analyses in this paper using the R programming language³⁷, using data.table³⁸ and metR³⁹ packages. Significant processing was performed using the CDO command line operators⁴⁰. All graphics are made using ggplot2⁴¹. The paper was rendered using knitr and Quarto^{42;43}.

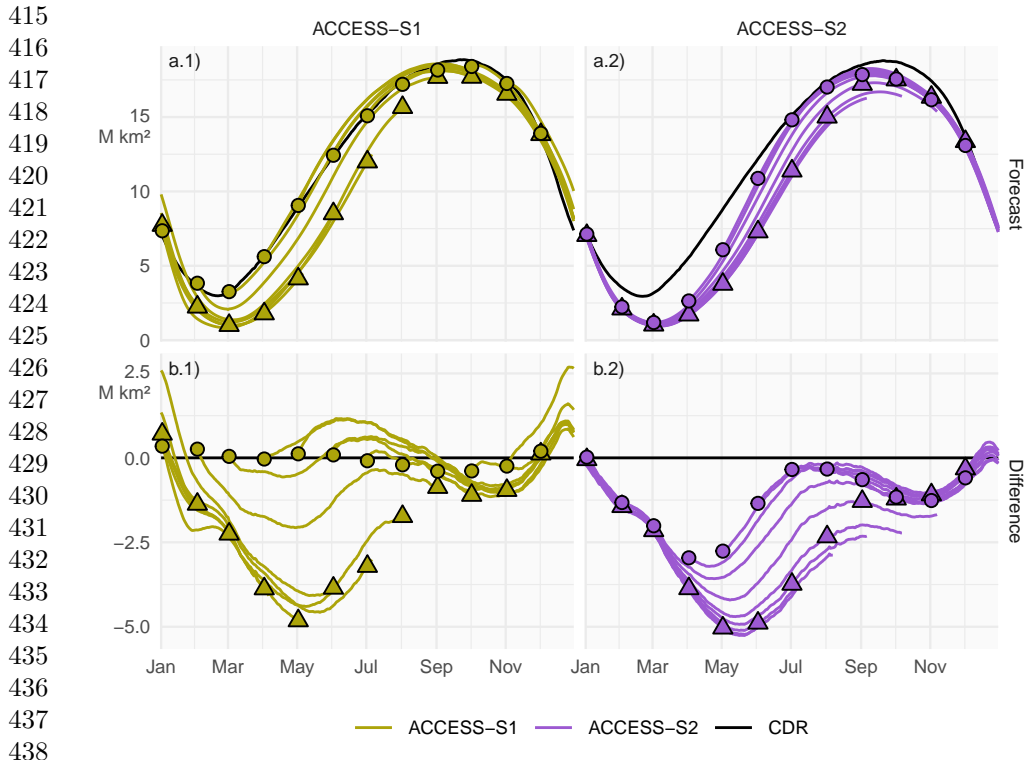
Results and discussion

371
372
373
374
375
376
377
378
379
380
381
382
383
384
385
386
387
388
389
390
391
392
393
394
395
396
397
398
399
400
401
402
403
404
405
406
407
408
409
410
411
412
413
414

Bias

Figure 1 (Figure A1 for OSI) shows mean sea-ice extent of the ACCESS-S1 and ACCESS-S2 hindcasts (row a) and their differences from mean sea-ice extent of NOAA/NSIDC CDRV4 (row b). Mean extent at the first of every month is indicated with circles for the initial conditions and with triangles for the longest lead time possible for each model (between 274 and 277 days for ACCESS-S2 and between 213 and 216 days for ACCESS-S1). At this long lead time, information of the initial conditions is essentially lost and the forecast reverts close to each model's preferred equilibrium state.

ACCESS-S2 initial conditions (circles in Fig. 1 column 2) show an overall negative bias, especially in the late summer-early autumn, while ACCESS-S1 initial conditions (circles in Fig. 1 column 1) are very close to observations, as expected from the assimilation of sea-ice observations to produce the initial conditions of ACCESS-S1. Both systems' equilibrium states (triangles) show negative biases of sea-ice extent, particularly in the growth phase of late-autumn and winter months. This is due primarily to the melt season being longer than in observations and with faster melt between January and March and the growing seasons being shorter with slower growth during March and April. This is then followed by faster growth between May and July (Figure 2 and



439 **Figure 1:** Row a: Pan-Antarctic daily mean sea-ice extent for all hindcasts initialised
 440 on the first of each calendar month for ACCESS-S1 (column 1; green) and ACCESS-S2
 441 (column 2; purple). Observed mean sea-ice extent in each corresponding hindcast period
 442 is shown in black. Row b: Mean differences between the forecast and the observed
 443 values. Circles represent the initial conditions at the start of forecasts (i.e., the first of
 444 every month), and triangles represent the mean values at the lead time corresponding
 445 to the maximum lead time in S1 (between 213 and 216 days, depending on the month)
 446
 447

448 Figure A2). Many sea-ice models exhibit this systematic underestimation during the
 449 sea-ice minimum and early freezing season⁸, which could indicate problems in the
 450 representation of thermodynamics in the model⁶. It is also not surprising that both
 451 forecasting systems converge to a similar equilibrium state because they share the
 452 same model formulation.
 453

454 The difference between the initial conditions (circles) and the model equilibrium
 455 state (triangles) can be mostly attributed to the effect of data assimilation, which
 456
 457

in ACCESS-S2 is due solely to the coupling of sea-ice with the atmosphere and the ocean. From May to October, in ACCESS-S2 circles are closer to observations than the triangles are, indicating that the information from the ocean and atmosphere data assimilation is affecting sea ice and improving the initial conditions. During these months, ACCESS-S1 can overestimate the sea-ice extent at short lead time. For the rest of the year circles are overlaid with triangles in ACCESS-S2, indicating that the ocean and atmosphere data assimilation is not affecting sea ice and that this component of the model is virtually free-running.

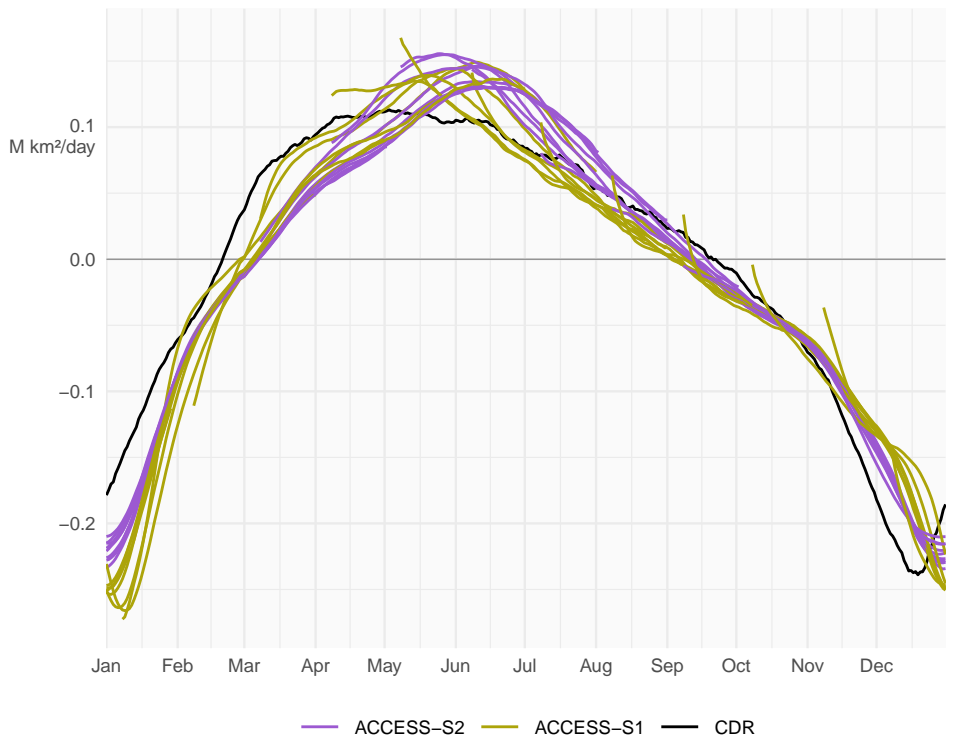
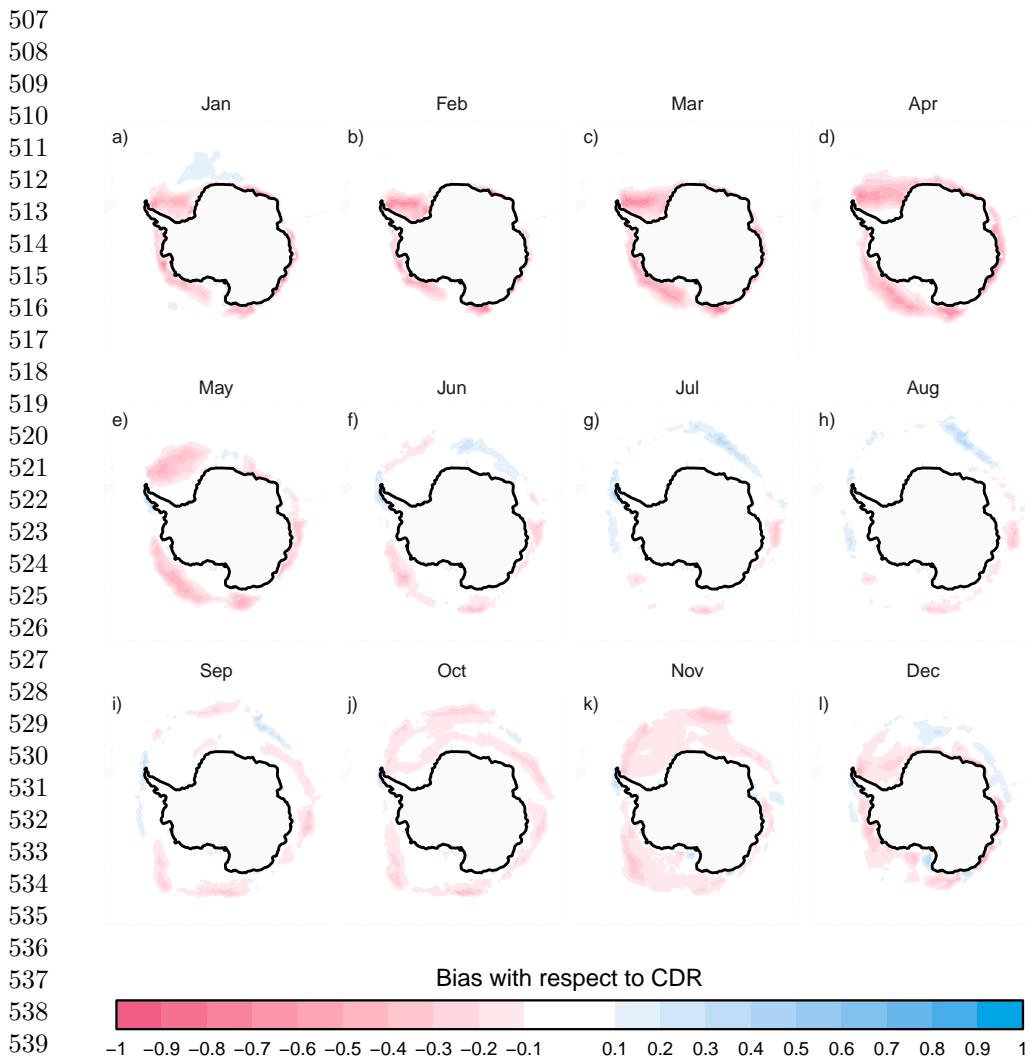


Figure 2: Mean daily sea-ice extent growth ($10^6 \text{ km}^2/\text{day}$) in ACCESS-S1 (green) and ACCESS-S2 (purple) hindcasts and observations (black), computed as the mean daily differences in sea-ice extent between each date and the next for each forecast month. Values are smoothed with a 11-day running mean.

461
462
463
464
465
466
467
468
469
470
471
472
473
474
475
476
477
478
479
480
481
482
483
484
485
486
487
488
489
490
491
492
493
494
495
496
497
498
499
500
501
502
503
504
505
506



543 **Figure 3:** Ensemble mean difference between monthly sea-ice concentration of
 544 ACCESS-S2 ensemble mean forecast at 0-month lead time (monthly mean values fore-
 545 casted from the forecast initialised at the first of the month) and observations (CDR).

546
 547 To further understand the bias in ACCESS-S2, Figure 3 (Figure A3) shows spatial pat-
 548 terns of the differences of monthly mean sea-ice concentrations between NOAA/NSIDC
 549 CDRV4 and ACCESS-S2 hindcasts at the shortest monthly lead time. From October
 550
 551
 552

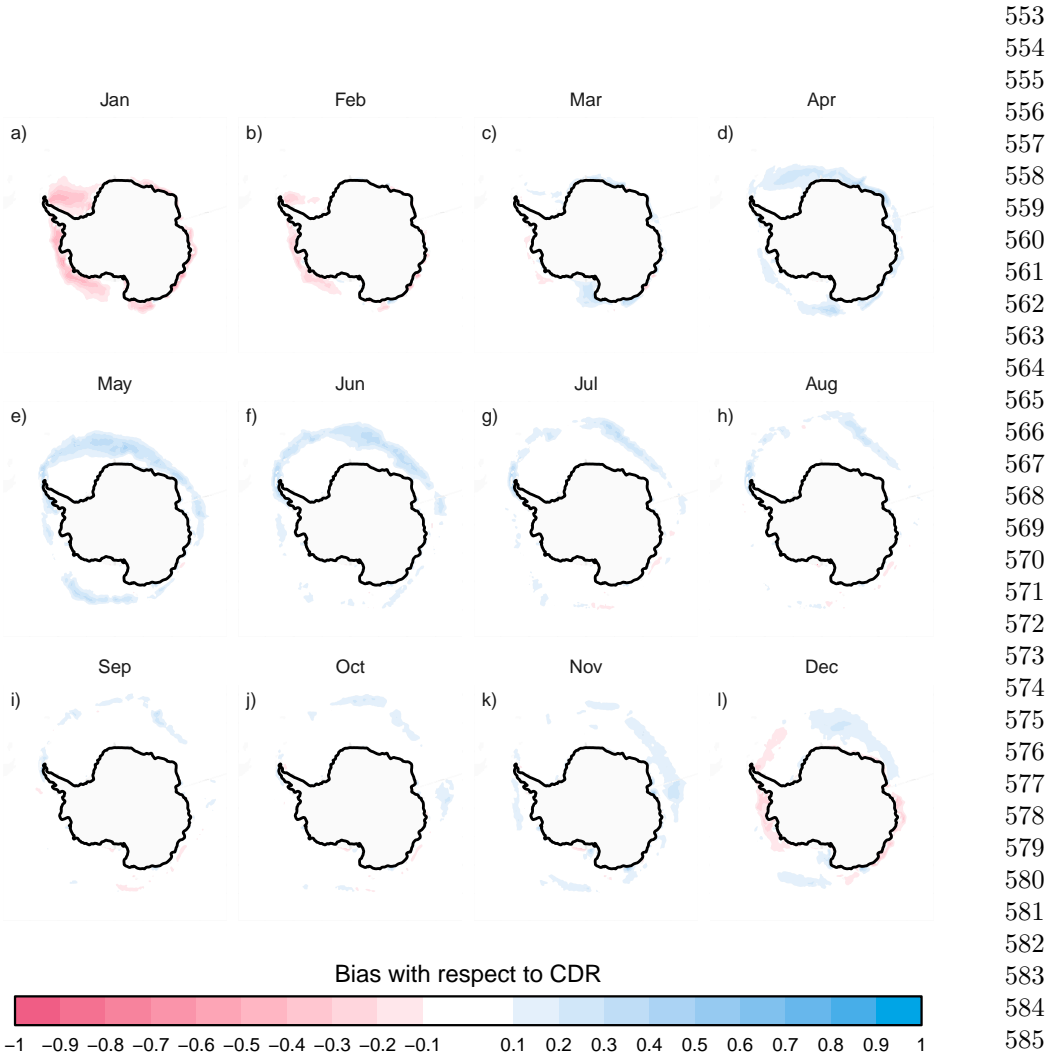


Figure 4: Same as Figure 3 but for ACCESS-S1.

to May, the model underestimates sea-ice concentrations in most regions except for the inner Weddell Sea in April and May, where sea-ice concentrations saturate to 1 both in the observations and forecasts. In winter, the differences are limited to a narrow band around the sea-ice edge with slight positive biases in the African sector

599 of East Antarctica and negative biases around the Indian Ocean sector which partially
600 compensate, resulting in the near-zero extent bias seen in those months (Figure 1).
601

602 ACCESS-S1 has a comparatively smaller overall bias (Figure 4 and Figure A4). The
603 largest values are found between April and June, when the faster growth results in
604 large positive bias along the sea-ice edge, and in January, when the faster melt leads
605 to large negative bias in the Weddell and Amundsen Seas.
606

607

608 **RMSE**

609

610

611 Figure 5 (Figure A5) shows monthly sea-ice extent anomalies forecasted at selected lead
612 times. Compared with ACCESS-S1, ACCESS-S2 anomaly forecasts are relatively poor
613 (large RMSE) even for the first month (lead time 0), whereas ACCESS-S1 forecasts
614 stay relatively skilful even at a lead time of three months. ACCESS-S2 shows much
615 larger interannual variability than observations, with dramatic lows between 1995 and
616 2007, and highs between 2007 and 2015.
617

618

619 Unexpectedly, for ACCESS-S2, RMSE improves with lead time, even though the
620 correlation degrades with lead time. This is puzzling behaviour that goes contrary to
621 what is usually seen in prediction models. The explanation seems to be the mentioned
622 increased interannual variability. Figure 6 (Figure A6) shows the interannual standard
623 deviation of monthly sea-ice extent of the forecasts as a function of lead time compared
624 with observations. ACCESS-S1 standard deviation lies within the observed standard
625 deviation regardless of lead time, while ACCESS-S2 standard deviation is more than
626 twice that of observations at zero lead time and only approaches the observed value at
627 nine month lead time for most months.
628

629

630 ACCESS-S2 forecasts of sea-ice extent anomalies seem to align moderately well
631 with observations (leading to moderately high correlation) but their magnitude is
632 overestimated (leading to large errors). This could be caused by ACCESS-S2 sea ice
633

634

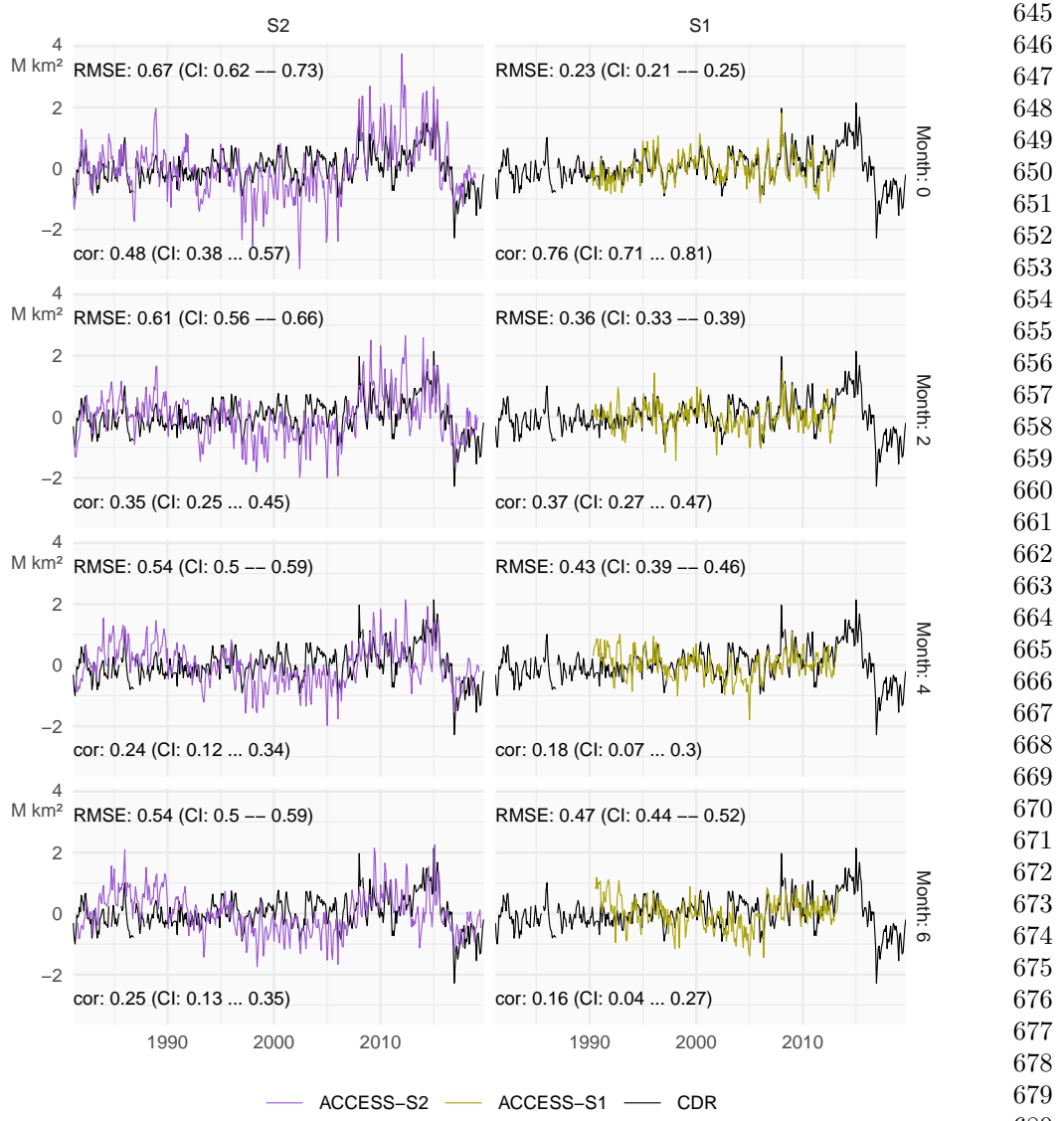


Figure 5: Monthly mean sea-ice extent anomalies of the observations (black) and forecasts from ACCESS-S1 (right column; purple) and ACCESS-S2 (left column; green) at lead times of 0, 2, 4, and 6 months. The RMSE and correlation during the overlapping period of ACCESS-S1 and ACCESS-S2 hindcasts (1990–2013) are shown on the top left and bottom left of each panel respectively.

being much more sensitive to atmospheric and oceanic forcing, perhaps due to lower thickness.

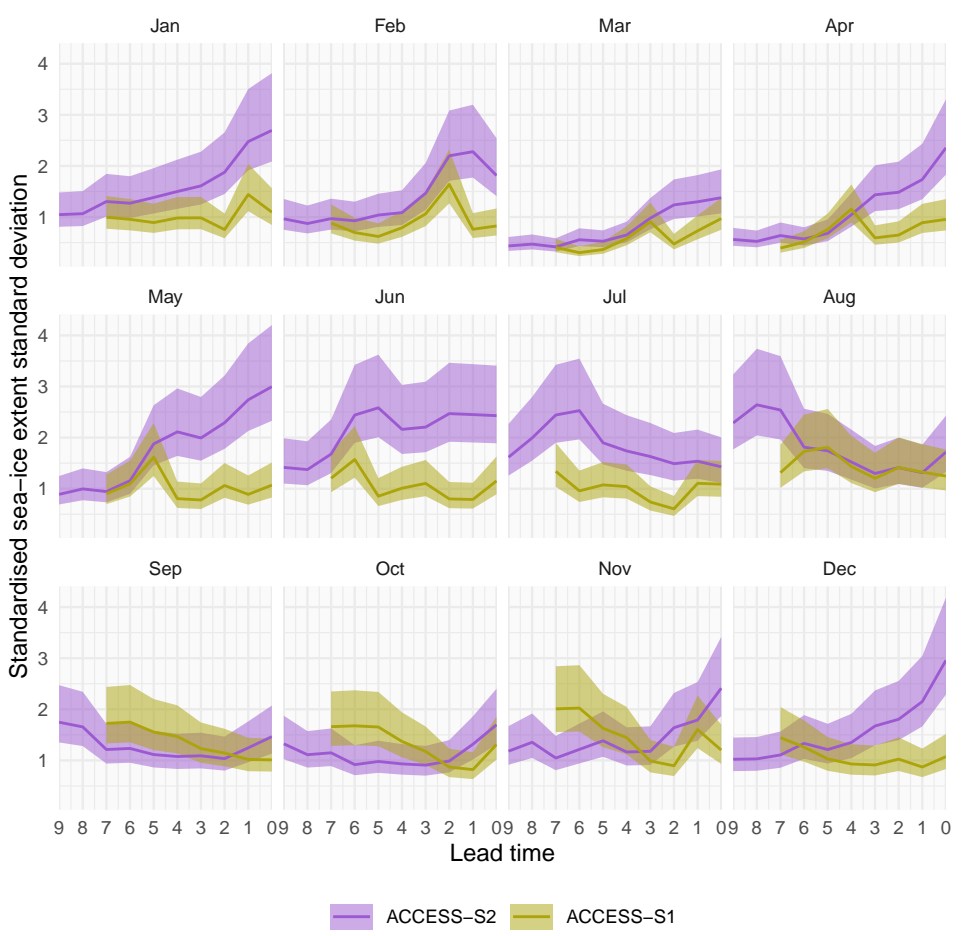


Figure 6: Interannual standard deviation with 95% confidence interval of monthly mean sea-ice extent forecasted for each month divided by that month's sea-ice extent observation standard deviation. ACCESS-S1 and ACCESS-S2 at different lead times. Each panel indicates the target month. Note the reverse horizontal axis.

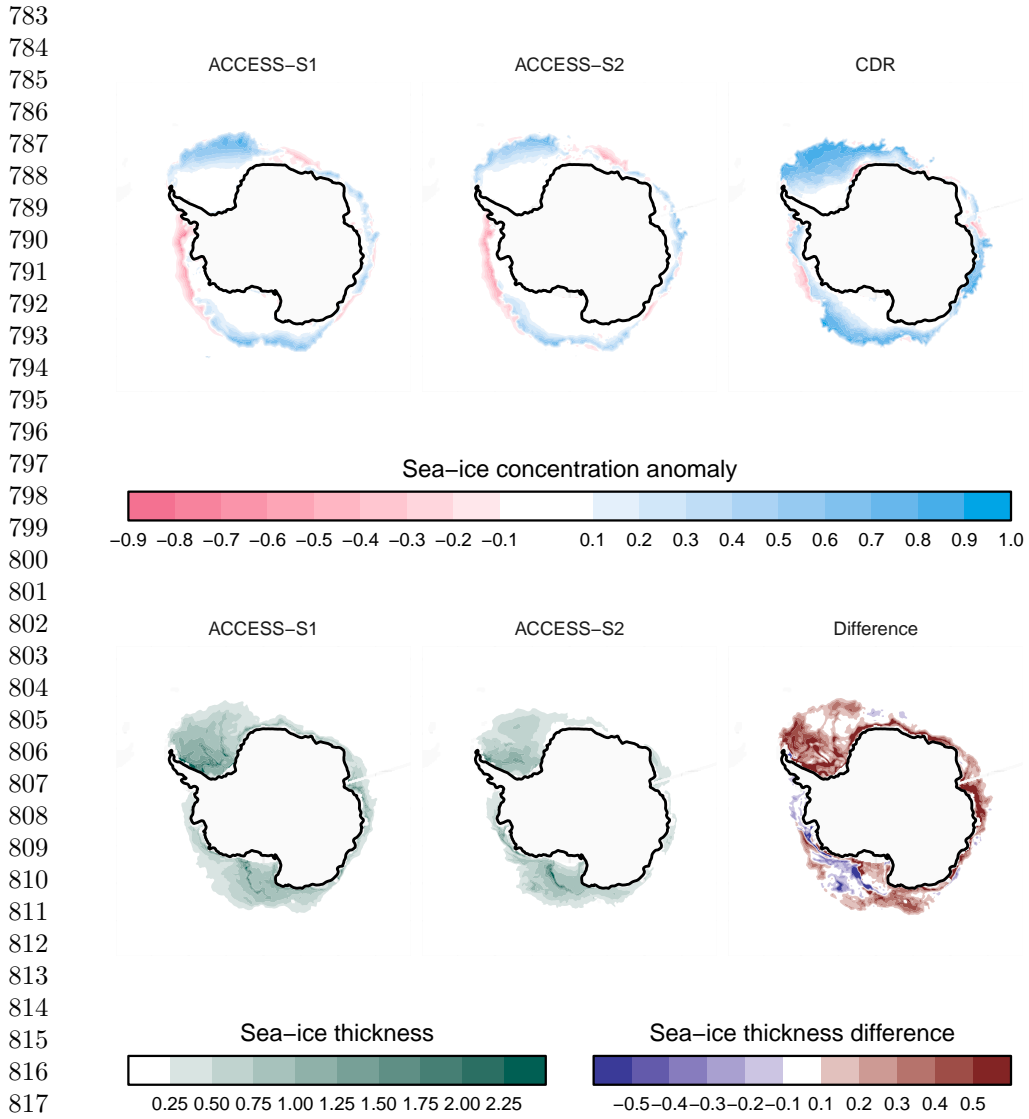
As an example, Figure 7 shows sea-ice concentration anomalies (top row) and sea-ice thickness and the difference between the two models (bottom row) for 2 May 2008 initialised one day prior; being that close to initialisation date, these are very approximately the initial conditions. ACCESS-S1 sea-ice concentrations anomalies are very close to observations as expected from the system assimilating these data. ACCESS-S2 sea-ice concentration anomalies, which are not assimilated, are not as

close, but the large-scale pattern is aligned with observations. The system simulates
large positive anomalies in the Weddell and Ross Seas and slight negative anomalies
in the Amundsen and Bellingshausen Seas. The fact that ACCESS-S2 can simulate
this pattern without assimilating sea-ice data suggests that atmospheric and oceanic
forcing were the dominant drivers. However, the magnitude of the sea-ice anomalies is
too big. It is plausible that this is due to the thinner ice simulated by ACCESS-S2
(bottom row).

Extending beyond the one case in Figure 7, Figure 8 (Figure ??) shows monthly
mean sea-ice thickness as a function of lead time for ACCESS-S1 and ACCESS-S2.
Supporting the idea that thinner ice is what causes the increased extent variability in
ACCESS-S2, this system simulates thinner sea-ice compared to ACCESS-S1 overall
at almost all lead times and in all months except for summer at short lead times
(Dec-Jan, 0-1 months; Feb-Mar, 0-2 months). However, in both systems, forecasted
sea-ice is thicker at shorter lead times and then decreases, particularly in the summer
months. If thinner ice were a sufficient cause of increased variability, then we would
expect variability to increase with lead time in both forecasting systems.

The fact that ACCESS-S1 and ACCESS-S2 share the same model configuration and
that the increased variability is more extreme at short lead times (Fig. 6) suggests
that the data assimilation procedure is partly responsible. It is possible that sea-ice in
the ACCESS-S2 system is left in an unbalanced state after assimilating atmospheric
and oceanic data but not sea-ice data, leading to large responses that are amplified
by the thin ice in the initial states which then subside at longer lead times when the
model is balanced.

To assess ACCESS-S2 forecasts in more detail, we compute error measures for all
hindcasts started on the 1st of every month. Figure 9 (Figure A7) shows the mean
RMSE of sea-ice concentration anomalies for ACCESS-S1 and ACCESS-S2 hindcasts
compared against persistence and climatological forecasts used as a benchmark. Due to



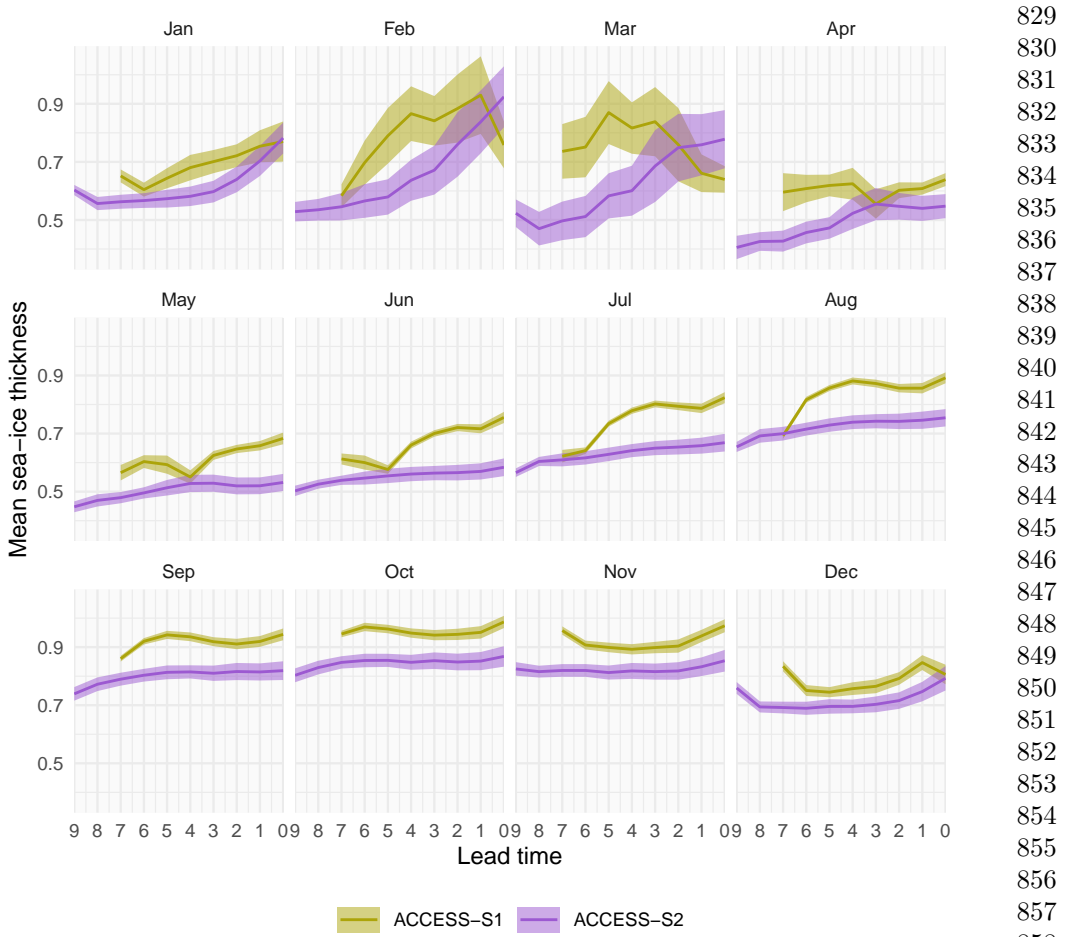
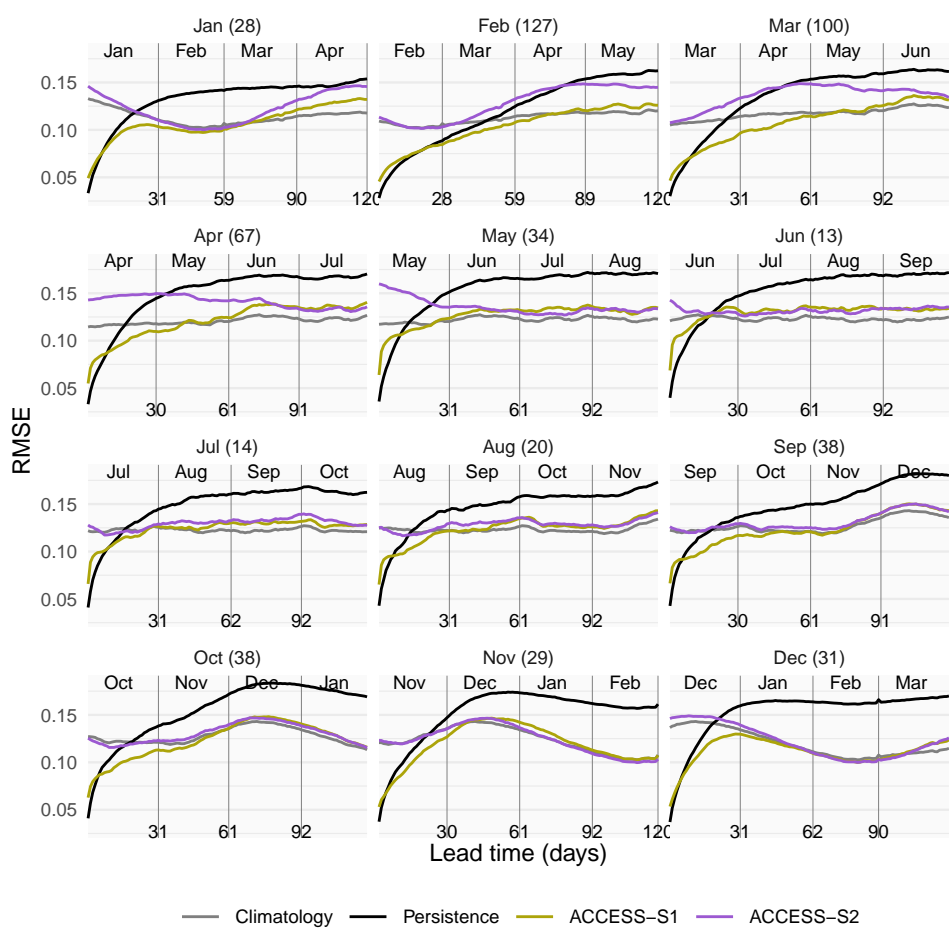


Figure 8: Mean and 95% interval of monthly mean sea-ice thickness for ACCESS-S1 and ACCESS-S2 at different lead times. Each panel indicates the target month. Note the reverse horizontal axis.

errors would grow faster and may eventually surpass the model forecast errors. The black line shows that the persistence forecast error indeed grows rapidly and reaches its maximum in about 30 days for most months except for February, when it grows much slower. The ACCESS-S1 forecast errors grow slower than persistence forecast errors and remain lower after less than 10 days on average. The ACCESS-S2 forecast error starts



905 **Figure 9:** Mean RMSE of sea-ice concentration anomalies as a function of forecast
 906 lead time for all forecasts initialised on the first of each month compared with a
 907 reference forecast of persistence of anomalies (black) and climatology (gray). Only the
 908 first 120 days are shown. In parentheses, the shortest time at which ACCESS-S1 and
 909 ACCESS-S2 mean RMSE is not statistically different at the 99% confidence level.

910
 911
 912 high in all months and is lower than the persistence forecast error after more than 15
 913 days in most months except for forecast initialised in February, when it takes 80 days.
 914

915
 916 At longer lead times, it is more appropriate to compare errors with the climatological
 917 forecast error. The lead time at which ACCESS-S1 forecast error is higher than
 918 the climatological forecast error varies between more than 60 and less than 20 days
 919

depending on forecast initialisation month with the minimum in June. ACCESS-S2	921
forecasts never have lower error than climatology, on the other hand, except marginally	922
in October forecasts.	923
	924
	925
	926
Figure 10 (Figure A8) summarises the lead time window in which each hindcast is	927
better than both the persistence forecast and the climatological forecast as a function	928
of forecast month. ACCESS-S1 forecasts have a wider lead time window in the summer	929
than the other seasons and is not better than both benchmarks at forecasting June	930
sea-ice concentration anomalies. Forecasts initialised in May and June are particularly	931
poor, and July cannot be forecasted better than the benchmarks. This is consistent	932
with the mid-winter loss of predictability observed by Libera et al. ⁴⁴ , who attributed	933
it to deep warm water entraining into the mixed layer.	934
	935
	936
	937
	938
	939
To analyse the spatial distribution of the model error, we computed the RMSE of	940
zonal mean sea-ice concentration anomalies on 15 slices of 24° longitude span for each	941
forecasting system. We control for some areas being naturally easier to forecast than	942
others by computing the RMSE skill score with the climatological forecast RMSE as	943
reference.	944
	945
	946
	947
	948
For ACCESS-S1 forecasts (Figure 11 and Figure A9), skill tends to be lower off the	949
coast of Eastern Antarctica even at short lead times; for instance, the skill score for	950
forecasts initialised in May and June are negative between 0° and 120°E even at almost	951
zero lead time. This mirrors Libera et al. ⁴⁴ findings of a “winter predictability barrier”,	952
although they focus on the Weddell Sea and here we show that the effect seems to be	953
stronger more to the east. In West Antarctica there is a hint of easterly-propagating	954
skill in forecasts initialised in February and March. This is consistent with Holland	955
et al. ¹³ findings that memory of sea-ice anomalies are stored in ocean heat content	956
anomalies that are transported east by the Antarctic Circumpolar Current.	957
	958
	959
	960
	961
	962
	963
	964
	965
	966

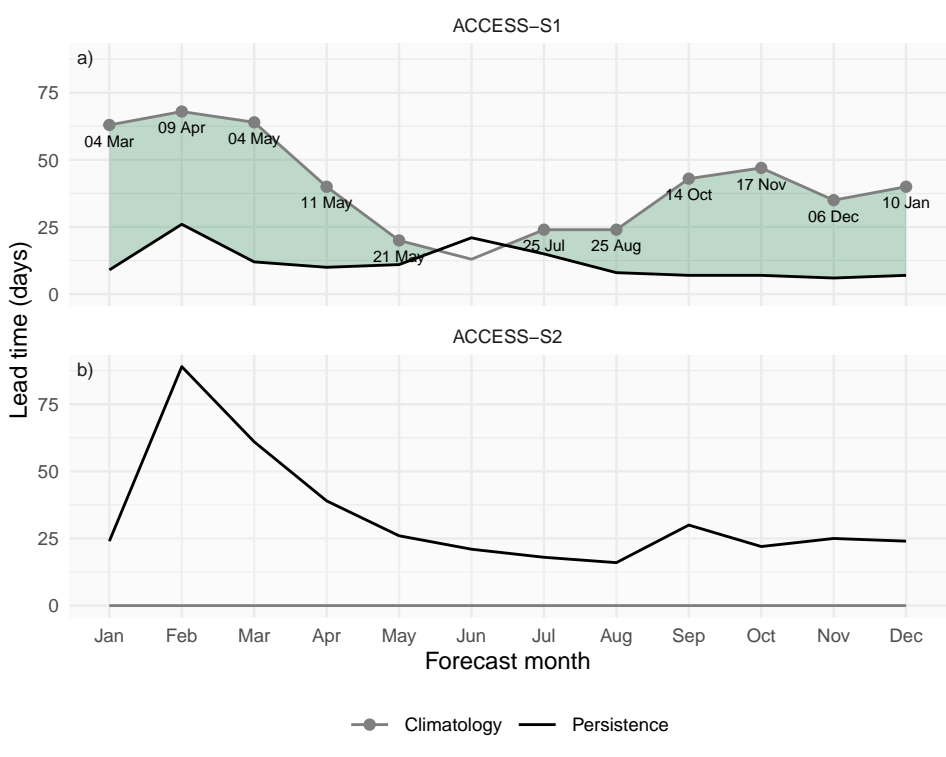


Figure 10: Minimum lead time at which each forecast's mean RMSE becomes larger than the lower bound of the 95% confidence interval of persistence forecast RMSE (black lines) and maximum lead time at which each forecast's mean RMSE remains lower than the lower bound of the 95% confidence interval of climatological forecast RMSE (gray lines). Green shading indicates the window where forecasts outperform both persistence (lead times longer than black line) and climatology (lead times shorter than gray line). Text labels show the date corresponding to the maximum lead time at which each forecast outperforms climatology.

ACCESS-S2 forecasts (Figure 12 and Figure A10) also have lower skill over East Antarctica. From July to December even though the pan-Antarctic average skill is negative at all lead times (Fig. 10), it is positive for up to a month in West Antarctica. Since oceanic and atmospheric forcing is the only source of information, this suggests that sea-ice in this region is particularly sensitive to oceanic and atmospheric forcing and suggests a role of the Pacific-South American mode and the Amundsen Sea Low to shape sea-ice concentration anomalies. The fact that this is evident in the

months in which El Niño–Southern Oscillation teleconnections are more important
for atmospheric circulation also suggests the influence of tropical Pacific variability.
February and March are the only two months that can be forecasted with marginally
positive skill in large regions.

Finally, Figure 13 (Figure A11) shows the difference in skill between ACCESS-S1
and ACCESS-S2. Large differences in skill indicate areas and months that are most
affected by the data assimilation present in ACCESS-S1. Between January and March,
which are the months in which ACCESS-S1 is the most skilful (Figure 10), most of
the improvement compared with ACCESS-S2 is present in the Ross and Weddell Sea.
In April and May, the improvement seems more homogeneous.

In Figure 9 the mean error was shown. Figure 14 (Figure A12) column 1 shows the mean
standard deviation of errors among ensemble members at various lead times. At one
day lead time (Fig. 14 a.1) ACCESS-S2 has a slightly larger spread than ACCESS-S1
due to the way that ensemble members are generated. ACCESS-S1 ensemble members
are generated by adding random field perturbations to the atmosphere only, which
then are transferred to the other components via the coupled simulation¹⁷. With this
scheme, ensemble members are all but guaranteed to be underdispersed in the ocean
and sea-ice components. The time-lag ensemble used for ACCESS-S2 ensures greater
spread. This difference is gone after about just two days, and both systems have a
comparable spread in ensemble member error afterwards (Fig. 14 b1 and c1).

Figure 14 column 2, on the other hand, shows the standard deviation of ensemble mean
error of each hindcast and the persistence forecast. At one day lead time, ACCESS-S2
ensemble mean error standard deviation is much larger than ACCESS-S1's, which in
turn is comparable to the persistence forecast error standard deviation. At longer lead
times, the spread of ACCESS-S1 and persistence forecast standard deviation increases
to eventually be comparable to ACCESS-S2 and the standard deviation in climatological

1059 forecast errors. ACCESS-S2 error standard deviation is fairly independent of lead time
1060 and similar to the climatological forecast error standard deviation at all lead times.
1061
1062
1063
1064
1065
1066
1067
1068
1069
1070
1071
1072
1073
1074
1075
1076
1077
1078
1079
1080
1081
1082
1083
1084
1085
1086
1087
1088
1089
1090
1091
1092
1093
1094
1095
1096
1097
1098
1099
1100
1101
1102
1103
1104

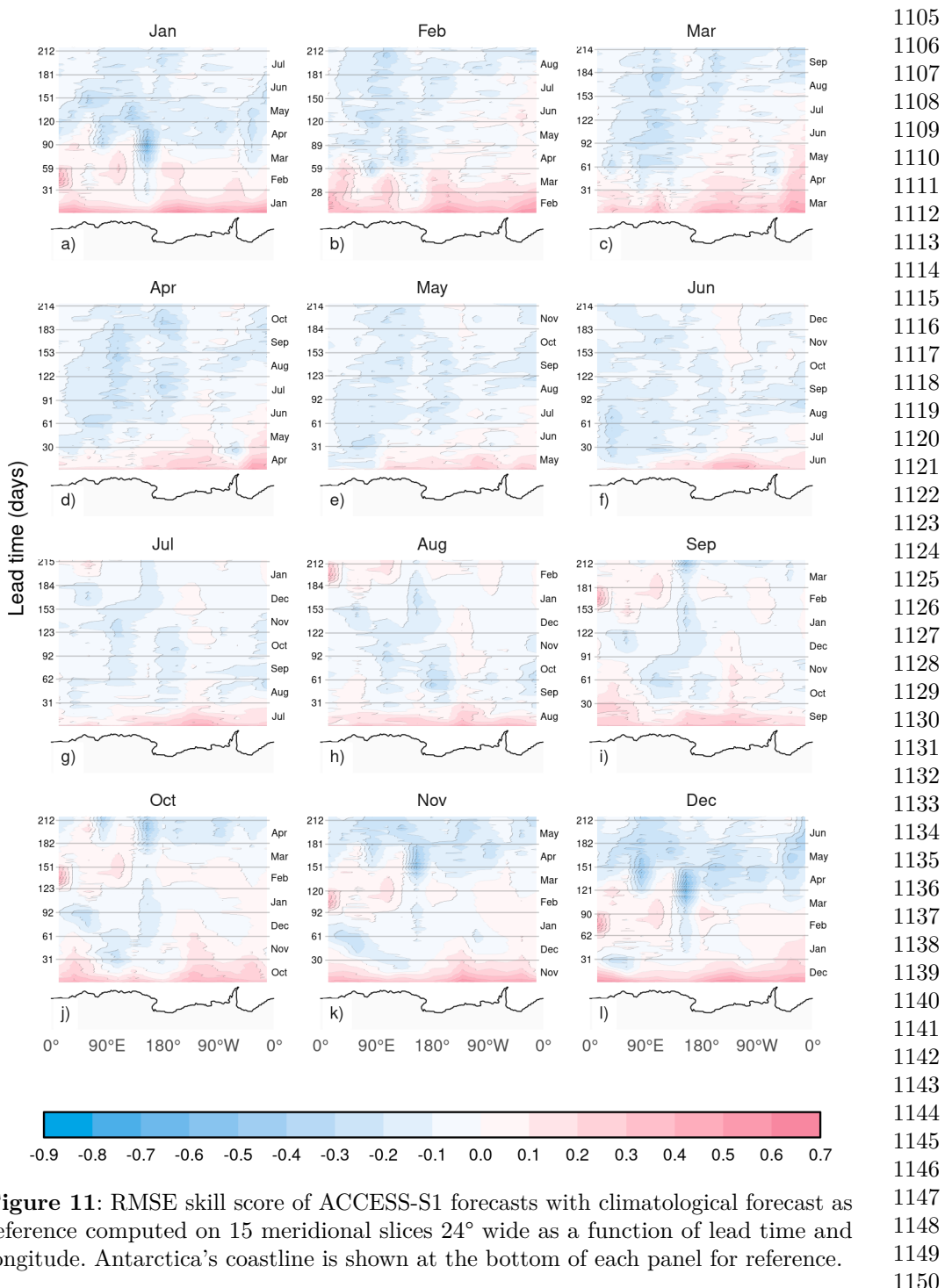


Figure 11: RMSE skill score of ACCESS-S1 forecasts with climatological forecast as reference computed on 15 meridional slices 24° wide as a function of lead time and longitude. Antarctica's coastline is shown at the bottom of each panel for reference.

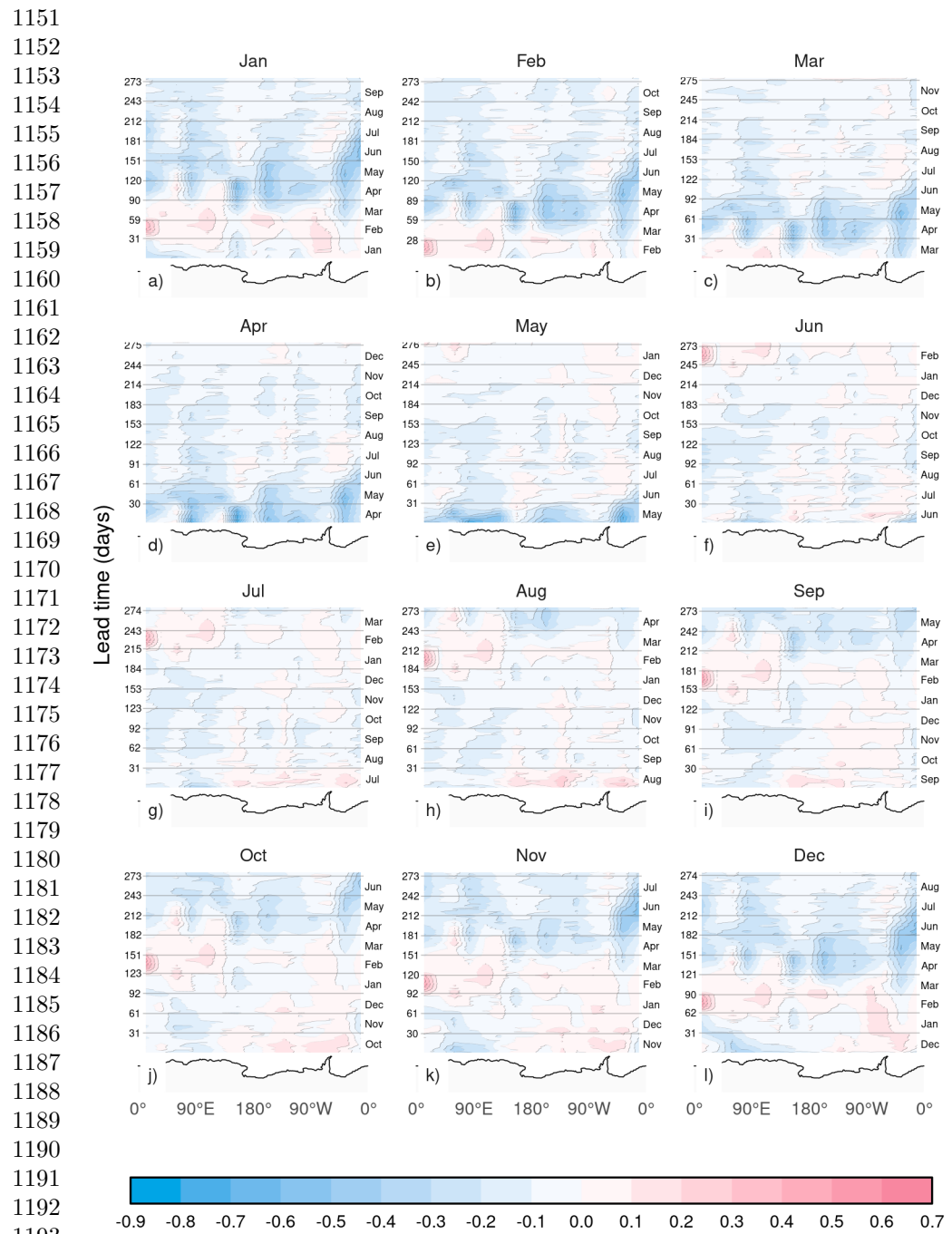


Figure 12: Same as Figure 11 but for ACCESS-S2.

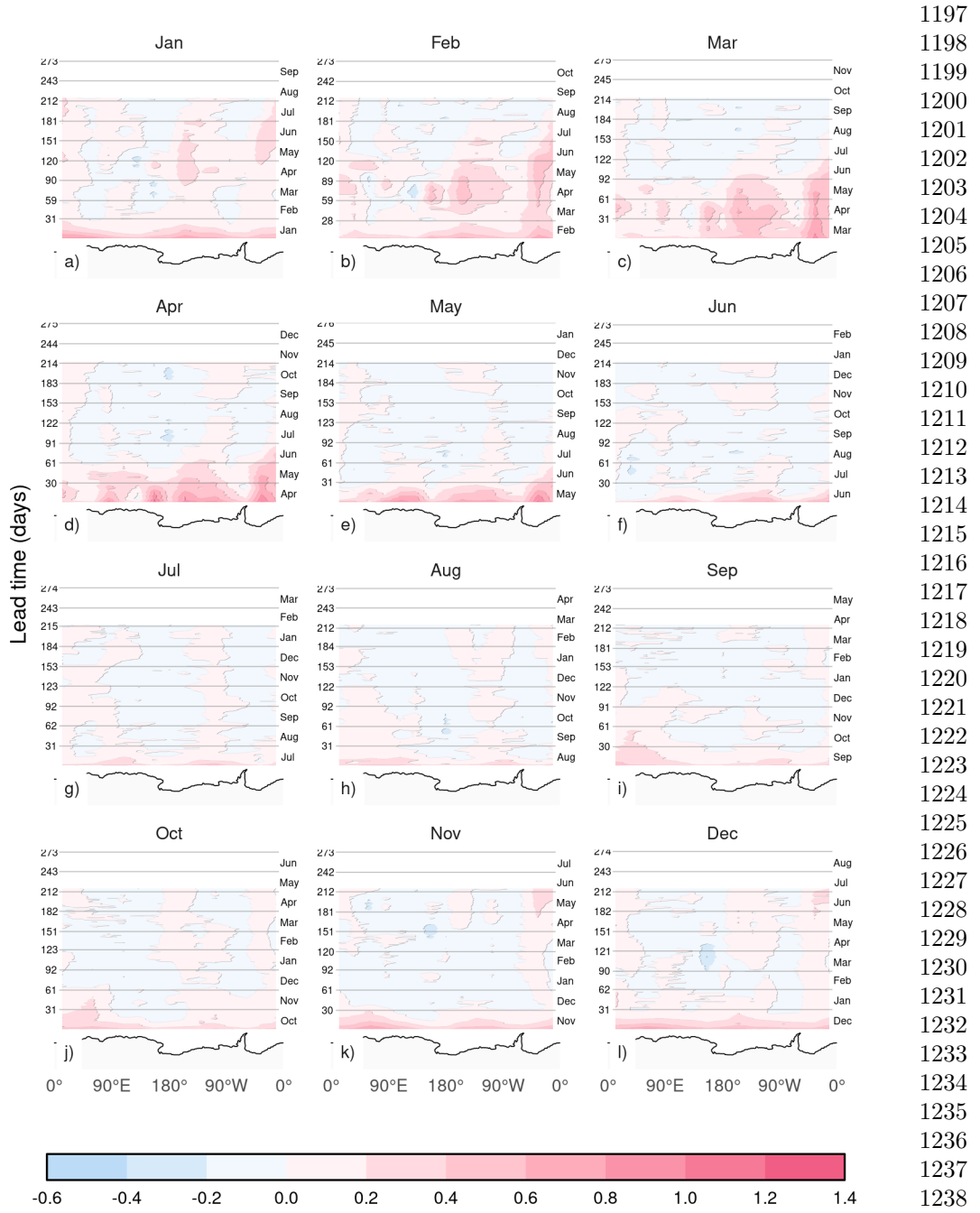
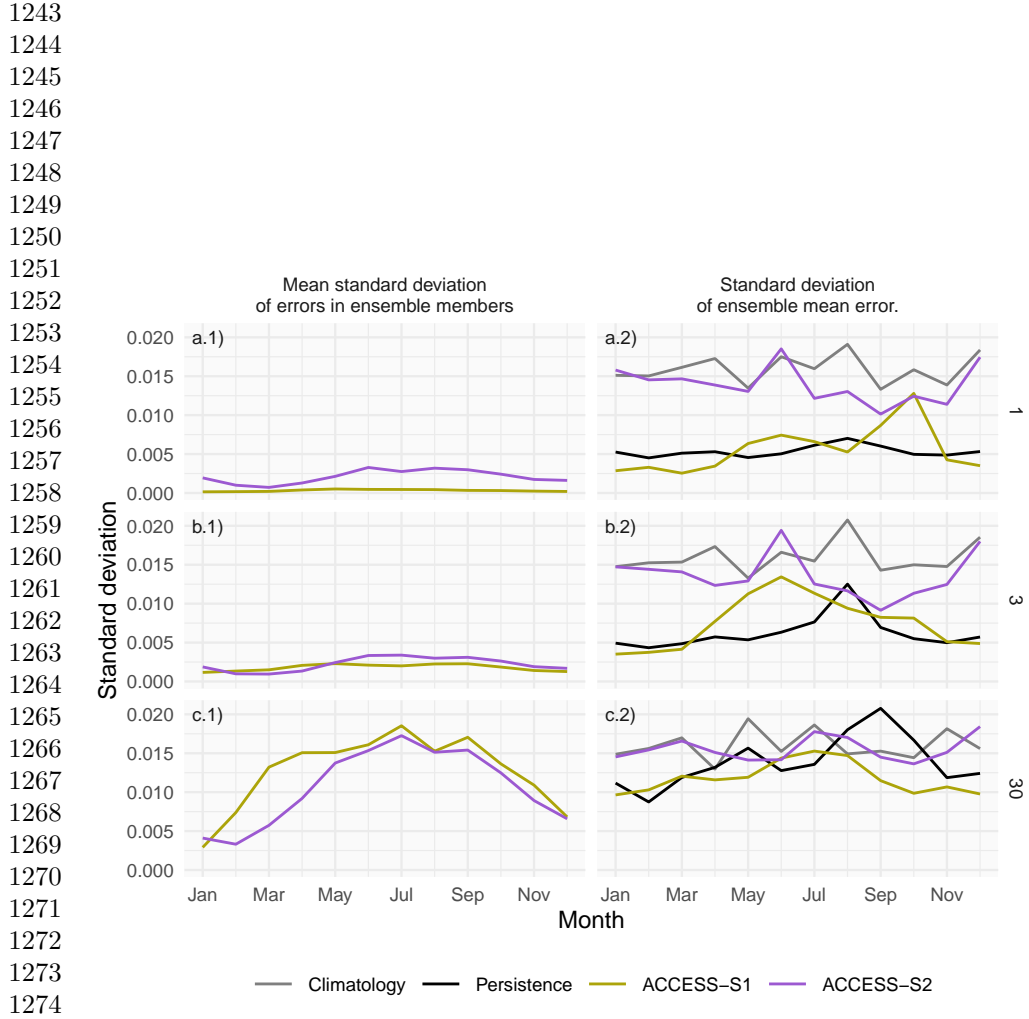


Figure 13: Same as Figure 11 but for the difference between ACCESS-S1 and ACCESS-S2.



1275 **Figure 14:** Decomposition of forecast error spread at 1, 5 and 30 days lead time for
 1276 ACCESS-S1 and ACCESS-S2 hindcasts across initialization months. The left column
 1277 shows the mean standard deviation of RMSE errors across ensemble members, while
 1278 the right column shows the standard deviation of the ensemble mean RMSE error and
 1279 the spread of the persistence and climatology forecasts errors.
 1280
 1281
 1282
 1283
 1284
 1285
 1286
 1287
 1288

Conclusions	1289
	1290
	1291
	1292
	1293
	1294
	1295
	1296
	1297
	1298
	1299
	1300
	1301
	1302
	1303
	1304
	1305
	1306
	1307
	1308
	1309
	1310
	1311
	1312
	1313
	1314
	1315
	1316
	1317
	1318
	1319
	1320
	1321
	1322
	1323
	1324
	1325
	1326
	1327
	1328
	1329
	1330
	1331
	1332
	1333
	1334
Sea-ice forecasts from the ACCESS-S2 system show a significant low extent bias, particularly during late summer and early autumn. This bias is attributed to a faster and longer melt season between January and March, and slower growth between March and April. This underestimation during the minimum and early freezing season is a common issue in many seasonal-to-subseasonal (S2S) systems, suggesting potential problems either with the model's thermodynamic representation or with short wave radiation forcing, as shown in other climate models ^{6;45} . Even though ACCESS-S2 shares the same model components as ACCESS-S1, the latter does not suffer from this bias, indicating that assimilating sea-ice concentrations successfully corrects for the negative bias that exists in the free-running model.	
Ensemble spread grows quickly even when perturbations are only implemented in the atmosphere component (in ACCESS-S1), indicating that sea ice is indeed responding quickly to atmospheric perturbations. However, our analysis suggests that the atmosphere and ocean data assimilation implemented in ACCESS-S2 is only effectively influencing sea-ice initial conditions from June to October, while the rest of the year, the sea-ice component runs virtually free, reverting to its biased equilibrium state. Zhou and Alves ⁴⁶ had previously evaluated sea-ice forecasts in ACCESS-S2 and also highlighted the poor performance of this forecasting system attributed to the lack of good initial conditions.	
Analysis of the error spread shows that ACCESS-S2 initial conditions from December to May not only have large errors, but that the initial error spread is very large compared with ACCESS-S1. This spread is not due to the perturbation scheme, since the mean error variance for individual forecasts is low and comparable with ACCESS-S1. Instead, it is due to large variance of the mean error of individual forecasts, which	

1335 is comparable to the climatology spread. This is further evidence that individual initial
1336 conditions are not being affected by the data assimilation scheme.
1337

1338
1339 Although ACCESS-S1 only assimilates sea-ice concentration, it is clear that sea-ice
1340 thickness is also affected through the assimilation process. ACCESS-S1 simulates
1341 significantly thicker ice than ACCESS-S2 and in both systems sea-ice is thicker at
1342 shorter lead times than at longer lead times. Both the explicit data assimilation in
1343 ACCESS-S2 and the effects of atmospheric and oceanic data assimilation in ACCESS-
1344 S1 might be nudging simulated sea ice to be thicker than the model equilibrium state.
1345
1346 We suggest that the thinner sea ice in ACCESS-S2 contributes to the large sea-ice
1347 extent variance, but other mechanisms, such as unbalanced initial conditions might
1348
1349 also be important.

1350
1351
1352 Given that ACCESS-S2 sea-ice extent is not directly initialised by sea-ice observations,
1353 comparing its forecasts with those of ACCESS-S1 allows us to estimate the time-
1354 scale over which initial conditions are important. We find that initial conditions affect
1355 Antarctic sea-ice forecasts in the order of a few months, but that effect is seasonally
1356 dependent. January to April initial conditions improve forecasts for up to three months.
1357 February initial conditions in particular are shown to be crucial for determining sea-ice
1358 evolution at least up to May. Arctic sea-ice forecasts also show greater sensitivity to
1359 initial conditions in boreal summer, compared with boreal winter^{12;47}, suggesting a
1360 similar mechanism might be playing a role.
1361

1362
1363 Forecasts initialised in winter have very little skill and ACCESS-S1 and ACCESS-S2
1364 forecast errors are statistically indistinguishable after just two weeks. This is consistent
1365 with Libera et al. ⁴⁴'s finding of a "winter predictability barrier" in the Weddell Sea,
1366 although they describe the barrier as a sharp loss of predictability in July, and here
1367 we find a gradual reduction in skill compared with climatology around June. This
1368 difference might be due to our use of pan-Antarctic RMSE, since our regional analysis
1369 indicates that the degraded skill is most dramatic in the King Haakon Sea.
1370

These findings have important implications for both operational forecasting, model development and predictability studies. For operational centers, our results suggest that efforts to improve sea-ice data assimilation should prioritize the summer and autumn months when initial conditions have the greatest impact on forecast skill. Additionally, the substantial bias in ACCESS-S2 highlights the need for improved model physics, particularly in the representation of sea-ice thermodynamics and radiation processes. Crucially, our results suggest dramatic seasonal variations in sea-ice predictability. Future studies should therefore use initial conditions through the whole year rather than focusing on a limited number of initialisation dates.	1381 1382 1383 1384 1385 1386 1387 1388 1389 1390 1391 1392 1393 1394 1395 1396 1397 1398 1399 1400 1401 1402 1403 1404 1405 1406 1407 1408 1409 1410 1411 1412 1413 1414 1415 1416 1417 1418 1419 1420 1421 1422 1423 1424 1425 1426
Funding	
This work was supported by ARC SRIEAS Grant SR200100005 Securing Antarctica's Environmental Future.	
Acknowledgments	
We thank the internal reviewers Bethan White and Xiaobing Zhou for their comments and feedback.	
This work benefited from earlier unpublished work by Laura Davies, Phil Reid, Andrew G. Marshall.	
This research was undertaken with the assistance of resources from the National Computational Infrastructure (NCI Australia), an NCRIS enabled capability supported by the Australian Government.	

1427 **Code and data availability**

1428

1429

1430 The underlying code for this study is available on GitHub:

1431 https://github.com/eliocamp/access-s2_ice-eval.

1433

1434 Raw data of ACCESS-S1 and ACCESS-S2 hindcast are not available due
1435 to size. Derived datasets required to reproduce the results, including extent

1436 timeseries and error measures, are available in this Zenodo repository:
1438

1439 <https://zenodo.org/records/17479538>⁴⁸

1440

1441

1442 **Competing interests**

1443

1444

1445 All authors declare no financial or non-financial competing interests.

1446

1447

1448

1449 **Author contributions**

1450

1451

1452 EC performed the data analysis and wrote the manuscript draft. AP, JA, EL, MW
1453 and PR, performed interpretation of the results, and reviewed and edited the draft.

1454

1455 All authors read and approved the final manuscript.

1456

1457

1458

1459 **References**

1460

1461

1462 [1] De Silva, L.W.A., Inoue, J., Yamaguchi, H., Terui, T.: Medium range sea ice
1463 prediction in support of Japanese research vessel MIRAI's expedition cruise in
1464 2018. Polar Geography **43**(2-3), 223–239 (2020) <https://doi.org/10.1080/1088937X.2019.1707317>

1465

1466 [2] Wagner, P.M., Hughes, N., Bourbonnais, P., Stroeve, J., Rabenstein, L., Bhatt,
1467 U., Little, J., Wiggins, H., Fleming, A.: Sea-ice information and forecast needs
1468

1469

1470

1471

1472

- for industry maritime stakeholders. *Polar Geography* **43**(2-3), 160–187 (2020) 1473
<https://doi.org/10.1080/1088937X.2020.1766592> 1474
- [3] Rinke, A., Maslowski, W., Dethloff, K., Clement, J.: Influence of sea ice on the 1475 atmosphere: A study with an Arctic atmospheric regional climate model. *Journal* 1476
of Geophysical Research: Atmospheres **111**(D16) (2006) <https://doi.org/10.1029/2005JD006957> 1477
- [4] Wang, Z., Fraser, A.D., Reid, P., Coleman, R., O'Farrell, S.: The Influence of 1478 Time-Varying Sea Ice Concentration on Antarctic and Southern Ocean Numerical 1479 Weather Prediction. *Weather and Forecasting* **39**(2), 293–310 (2024) <https://doi.org/10.1175/WAF-D-22-0220.1>. Chap. *Weather and Forecasting* 1480
- [5] Semmler, T., Kasper, M.A., Jung, T., Serrar, S.: Remote impact of the Antarctic 1481 atmosphere on the southern mid?latitudes. *Meteorologische Zeitschrift* **25**(1), 1482
71–77 (2016) <https://doi.org/10.1127/metz/2015/0685> 1483
- [6] Zampieri, L., Goessling, H.F., Jung, T.: Predictability of Antarctic Sea Ice Edge 1484 on Subseasonal Time Scales. *Geophysical Research Letters* **46**(16), 9719–9727 1485
(2019) <https://doi.org/10.1029/2019GL084096> 1486
- [7] Gao, Y., Xiu, Y., Nie, Y., Luo, H., Yang, Q., Zampieri, L., Lv, X., Uotila, P.: An Assessment of Subseasonal Prediction Skill of the Antarctic Sea Ice 1487 Edge. *Journal of Geophysical Research: Oceans* **129**(11), 2024–021499 (2024) 1488
<https://doi.org/10.1029/2024JC021499> 1489
- [8] Massonnet, F., Barreira, S., Barthélémy, A., Bilbao, R., Blanchard-Wrigglesworth, E., Blockley, E., Bromwich, D.H., Bushuk, M., Dong, X., Goessling, H.F., Hobbs, W., Iovino, D., Lee, W.-S., Li, C., Meier, W.N., Merryfield, W.J., Moreno-Chamarro, E., Morioka, Y., Li, X., Niraula, B., Petty, A., Sanna, A., Scilingo, M., 1490

- 1519 Shu, Q., Sigmond, M., Sun, N., Tietsche, S., Wu, X., Yang, Q., Yuan, X.: SIPN
1520 South: Six years of coordinated seasonal Antarctic sea ice predictions. *Frontiers*
1521 in Marine Science
- 1522 **10** (2023) <https://doi.org/10.3389/fmars.2023.1148899>
- 1523
- 1524
- 1525 [9] Dong, X., Yang, Q., Nie, Y., Zampieri, L., Wang, J., Liu, J., Chen, D.: Antarctic
1526 sea ice prediction with A convolutional long short-term memory network. *Ocean*
1527 *Modelling* **190**, 102386 (2024) <https://doi.org/10.1016/j.ocemod.2024.102386>
- 1528
- 1529
- 1530 [10] Lin, Y., Yang, Q., Li, X., Dong, X., Luo, H., Nie, Y., Wang, J., Wang, Y., Min,
1531 C.: Ice-kNN-South: A Lightweight Machine Learning Model for Antarctic Sea Ice
1532 Prediction. *Journal of Geophysical Research: Machine Learning and Computation*
1533 **2**(1), 2024–000433 (2025) <https://doi.org/10.1029/2024JH000433>
- 1534
- 1535
- 1536
- 1537
- 1538 [11] Guemas, V., Chevallier, M., Déqué, M., Bellprat, O., Doblas-Reyes, F.: Impact
1539 of sea ice initialization on sea ice and atmosphere prediction skill on seasonal
1540 timescales. *Geophysical Research Letters* **43**(8), 3889–3896 (2016) <https://doi.org/10.1002/2015GL066626>
- 1541
- 1542
- 1543
- 1544
- 1545 [12] Day, J.J., Hawkins, E., Tietsche, S.: Will Arctic sea ice thickness initialization
1546 improve seasonal forecast skill? *Geophysical Research Letters* **41**(21), 7566–7575
1547 (2014) <https://doi.org/10.1002/2014GL061694>
- 1548
- 1549
- 1550
- 1551 [13] Holland, M.M., Blanchard-Wrigglesworth, E., Kay, J., Vavrus, S.: Initial-value
1552 predictability of Antarctic sea ice in the Community Climate System Model 3.
1553 *Geophysical Research Letters* **40**(10), 2121–2124 (2013) <https://doi.org/10.1002/grl.50410>
- 1554
- 1555
- 1556
- 1557
- 1558 [14] Marchi, S., Fichefet, T., Goosse, H.: Respective influences of perturbed atmospheric
1559 and ocean–sea ice initial conditions on the skill of seasonal Antarctic sea ice
1560 predictions: A study with NEMO3.6–LIM3. *Ocean Modelling* **148**, 101591 (2020)
1561
- 1562
- 1563
- 1564

- <https://doi.org/10.1016/j.ocemod.2020.101591> 1565
1566
1567
1568
1569
1570
1571
1572
1573
1574
1575
1576
1577
1578
1579
1580
1581
1582
1583
1584
1585
1586
1587
1588
1589
1590
1591
1592
1593
1594
1595
1596
1597
1598
1599
1600
1601
1602
1603
1604
1605
1606
1607
1608
1609
1610
- [15] Morioka, Y., Iovino, D., Cipollone, A., Masina, S., Behera, S.K.: Decadal Sea Ice Prediction in the West Antarctic Seas with Ocean and Sea Ice Initializations. Communications Earth & Environment **3**(1), 189 (2022) <https://doi.org/10.1038/s43247-022-00529-z>
- [16] Wedd, R., Alves, O., Burgh-Day, C., Down, C., Griffiths, M., Hendon, H.H., Hudson, D., Li, S., Lim, E.-P., Marshall, A.G., Shi, L., Smith, P., Smith, G., Spillman, C.M., Wang, G., Wheeler, M.C., Yan, H., Yin, Y., Young, G., Zhao, M., Xiao, Y., Zhou, X.: ACCESS-S2: The upgraded Bureau of Meteorology multi-week to seasonal prediction system. Journal of Southern Hemisphere Earth Systems Science **72**(3), 218–242 (2022) <https://doi.org/10.1071/ES22026>
- [17] Hudson, D., Alves, O., Hendon, H.H., Lim, E.-P., Liu, G., Luo, J.-J., MacLachlan, C., Marshall, A.G., Shi, L., Wang, G., Wedd, R., Young, G., Zhao, M., Zhou, X.: ACCESS-S1 The new Bureau of Meteorology multi-week to seasonal prediction system. Journal of Southern Hemisphere Earth Systems Science **67**(3), 132–159 (2017) <https://doi.org/10.1071/es17009>
- [18] Williams, K.D., Harris, C.M., Bodas-Salcedo, A., Camp, J., Comer, R.E., Copsey, D., Fereday, D., Graham, T., Hill, R., Hinton, T., Hyder, P., Ineson, S., Masato, G., Milton, S.F., Roberts, M.J., Rowell, D.P., Sanchez, C., Shelly, A., Sinha, B., Walters, D.N., West, A., Woollings, T., Xavier, P.K.: The Met Office Global Coupled model 2.0 (GC2) configuration. Geoscientific Model Development **8**(5), 1509–1524 (2015) <https://doi.org/10.5194/gmd-8-1509-2015>
- [19] Waters, J., Bell, M.J., Martin, M.J., Lea, D.J.: Reducing ocean model imbalances in the equatorial region caused by data assimilation. Quarterly Journal of the Royal Meteorological Society **143**(702), 195–208 (2017) <https://doi.org/10.1002/qj.2912>

- 1611 [20] Best, M.J., Pryor, M., Clark, D.B., Rooney, G.G., Essery, R.L.H., Ménard, C.B.,
1612 Edwards, J.M., Hendry, M.A., Porson, A., Gedney, N., Mercado, L.M., Sitch,
1613 S., Blyth, E., Boucher, O., Cox, P.M., Grimmond, C.S.B., Harding, R.J.: The
1614 Joint UK Land Environment Simulator (JULES), model description – Part 1:
1615 Energy and water fluxes. *Geoscientific Model Development* **4**(3), 677–699 (2011)
1616
1617 <https://doi.org/10.5194/gmd-4-677-2011>
1618
1619
1620
1621
1622 [21] Gurvan, M., Bourdallé-Badie, R., Bouttier, P.-A., Bricaud, C., Bruciaferri, D.,
1623 Calvert, D., Chanut, J., Clementi, E., Coward, A., Delrosso, D., Ethé, C., Flavoni,
1624 S., Graham, T., Harle, J., Iovino, D., Lea, D., Lévy, C., Lovato, T., Martin,
1625 N., Masson, S., Mocavero, S., Paul, J., Rousset, C., Storkey, D., Storto, A.,
1626 Vancoppenolle, M.: NEMO ocean engine (2013) <https://doi.org/10.5281/zenodo.1475234>
1627
1628
1629
1630
1631
1632 [22] Megann, A., Storkey, D., Aksenov, Y., Alderson, S., Calvert, D., Graham, T.,
1633 Hyder, P., Siddorn, J., Sinha, B.: GO5.0: The joint NERC–Met Office NEMO
1634 global ocean model for use in coupled and forced applications. *Geoscientific Model
1635 Development* **7**(3), 1069–1092 (2014) <https://doi.org/10.5194/gmd-7-1069-2014>
1636
1637
1638
1639
1640 [23] Rae, J.G.L., Hewitt, H.T., Keen, A.B., Ridley, J.K., West, A.E., Harris, C.M.,
1641 Hunke, E.C., Walters, D.N.: Development of the Global Sea Ice 6.0 CICE configu-
1642 ration for the Met Office Global Coupled model. *Geoscientific Model Development*
1643
1644 **8**(7), 2221–2230 (2015) <https://doi.org/10.5194/gmd-8-2221-2015>
1645
1646
1647 [24] Dee, D.P., Uppala, S.M., Simmons, A.J., Berrisford, P., Poli, P., Kobayashi, S.,
1648 Andrae, U., Balmaseda, M.A., Balsamo, G., Bauer, P., Bechtold, P., Beljaars,
1649 A.C.M., van de Berg, L., Bidlot, J., Bormann, N., Delsol, C., Dragani, R., Fuentes,
1650 M., Geer, A.J., Haimberger, L., Healy, S.B., Hersbach, H., Hólm, E.V., Isaksen,
1651 L., Kållberg, P., Köhler, M., Matricardi, M., McNally, A.P., Monge-Sanz, B.M.,
1652
1653
1654
1655
1656

- Morcrette, J.-J., Park, B.-K., Peubey, C., de Rosnay, P., Tavolato, C., Thépaut, J.-N., Vitart, F.: The ERA-Interim reanalysis: Configuration and performance of the data assimilation system. *Quarterly Journal of the Royal Meteorological Society* **137**(656), 553–597 (2011) <https://doi.org/10.1002/qj.828> 1657
1658
1659
1660
1661
1662
1663
- [25] Waters, J., Lea, D.J., Martin, M.J., Mirouze, I., Weaver, A., While, J.: Implementing a variational data assimilation system in an operational 1/4 degree global ocean model. *Quarterly Journal of the Royal Meteorological Society* **141**(687), 333–349 (2015) <https://doi.org/10.1002/qj.2388> 1664
1665
1666
1667
1668
1669
1670
1671
- [26] Good, S.A., Martin, M.J., Rayner, N.A.: EN4: Quality controlled ocean temperature and salinity profiles and monthly objective analyses with uncertainty estimates. *Journal of Geophysical Research: Oceans* **118**(12), 6704–6716 (2013) <https://doi.org/10.1002/2013JC009067> 1672
1673
1674
1675
1676
1677
1678
1679
1680
- [27] Reynolds, R.W., Smith, T.M., Liu, C., Chelton, D.B., Casey, K.S., Schlax, M.G.: Daily High-Resolution-Blended Analyses for Sea Surface Temperature. *Journal of Climate* **20**(22), 5473–5496 (2007) <https://doi.org/10.1175/2007JCLI1824.1> .
Chap. *Journal of Climate* 1681
1682
1683
1684
1685
1686
- [28] Zweng, M.M., Reagan, J.R., Antonov, J.I., Locarnini, R.A., Mishonov, A.V., Boyer, T.P., Garcia, H.E., Baranova, O.K., Johnson, D.R., Seidov, D., Biddle, M.M.: World ocean atlas 2013. Volume 2, Salinity (2013) <https://doi.org/10.7289/V5251G4D> 1687
1688
1689
1690
1691
1692
1693
1694
1695
1696
1697
1698
1699
1700
- [29] Meier, W.N., Stewart, J.S.: Assessing uncertainties in sea ice extent climate indicators. *Environmental Research Letters* **14**(3), 035005 (2019) <https://doi.org/10.1088/1748-9326/aaf52c> 1701
1702

- 1703 NOAA/NSIDC passive microwave sea-ice concentration climate record. Polar
1704 Research (2014) <https://doi.org/10.3402/polar.v33.21004>
- 1705
- 1706
- 1707 [31] Cavalieri, D.J., Gloersen, P., Campbell, W.J.: Determination of sea ice parameters
1708 with the NIMBUS 7 SMMR. Journal of Geophysical Research: Atmospheres
1709 89(D4), 5355–5369 (1984) <https://doi.org/10.1029/JD089iD04p05355>
- 1710
- 1711
- 1712
- 1713 [32] Comiso, J.: Bootstrap Sea Ice Concentrations from Nimbus-7 SMMR and DMSP
1714 SSM/I-SSMIS. (NSIDC-0079, Version 4). NASA National Snow and Ice Data
1715 Center Distributed Active Archive Center., Boulder, Colorado USA. (2023). <https://doi.org/10.5067/X5LG68MH013O>
- 1716
- 1717
- 1718
- 1719
- 1720 [33] Meier, W.N., Fetterer, F., Windnagel, A.K., Stewart, J.S.: NOAA/NSIDC Climate
1721 Data Record of Passive Microwave Sea Ice Concentration. National Snow and Ice
1722 Data Center., Boulder, Colorado USA (2021). <https://doi.org/10.7265/efmz-2t65>
- 1723
- 1724
- 1725
- 1726 [34] EUMETSAT Ocean and Sea Ice Satellite Application Facility: Global
1727 Sea Ice Concentration Climate Data Record 1978-2020 (v3.0, 2022),
1728 OSI-450-a, <https://cds.climate.copernicus.eu/cdsapp#!/dataset/satellite-sea-ice-concentration>
- 1729
- 1730
- 1731
- 1732
- 1733
- 1734 [35] Cavalieri, D.J., Crawford, J.P., Drinkwater, M.R., Eppler, D.T., Farmer, L.D.,
1735 Jentz, R.R., Wackerman, C.C.: Aircraft active and passive microwave validation
1736 of sea ice concentration from the Defense Meteorological Satellite Program special
1737 sensor microwave imager. Journal of Geophysical Research: Oceans 96(C12),
1738 21989–22008 (1991) <https://doi.org/10.1029/91JC02335>
- 1739
- 1740
- 1741
- 1742
- 1743 [36] Murphy, A.H., Daan, H.: Forecast Evaluation. In: Probability, Statistics, And
1744 Decision Making In The Atmospheric Sciences. CRC Press, ??? (1985)
- 1745
- 1746
- 1747 [37] R Core Team: R: A Language and Environment for Statistical Computing. R
1748

Foundation for Statistical Computing, Vienna, Austria (2020). R Foundation for Statistical Computing	1749 1750 1751 1752
[38] Dowle, M., Srinivasan, A.: Data.Table: Extension of 'Data.Frame' (2020)	1753 1754
[39] Campitelli, E.: metR: Tools for Easier Analysis of Meteorological Fields (2020)	1755 1756 1757
[40] Schulzweida, U.: CDO User Guide (2023) https://doi.org/10.5281/ZENODO.10020800	1758 1759 1760 1761
[41] Wickham, H.: Ggplot2: Elegant Graphics for Data Analysis. Use R! Springer, New York (2009). https://doi.org/10.1007/978-0-387-98141-3	1762 1763 1764 1765
[42] Xie, Y.: Dynamic Documents with R and Knitr, 2nd edn. Chapman and Hall/CRC, Boca Raton, Florida (2015)	1766 1767 1768 1769
[43] Allaire, J.J., Teague, C., Xie, Y., Dervieux, C.: Quarto. Zenodo (2022). https://doi.org/10.5281/ZENODO.5960048	1770 1771 1772 1773
[44] Libera, S., Hobbs, W., Klocker, A., Meyer, A., Matear, R.: Ocean-Sea Ice Processes and Their Role in Multi-Month Predictability of Antarctic Sea Ice. Geophysical Research Letters 49 (8), 2021–097047 (2022) https://doi.org/10.1029/2021GL097047	1774 1775 1776 1777 1778 1779 1780 1781
[45] Roach, L.A., Dörr, J., Holmes, C.R., Massonnet, F., Blockley, E.W., Notz, D., Rackow, T., Raphael, M.N., O'Farrell, S.P., Bailey, D.A., Bitz, C.M.: Antarctic Sea Ice Area in CMIP6. Geophysical Research Letters 47 (9), 2019–086729 (2020) https://doi.org/10.1029/2019GL086729	1782 1783 1784 1785 1786 1787 1788 1789
[46] Zhou, X., Alves, O.: Evaluating sea ice in ACCESS-S2. Technical report, Bureau of Meteorology (2022)	1790 1791 1792 1793 1794

1795 [47] Bunzel, F., Notz, D., Baehr, J., Müller, W.A., Fröhlich, K.: Seasonal climate
1796 forecasts significantly affected by observational uncertainty of Arctic sea ice
1797 concentration. Geophysical Research Letters **43**(2), 852–859 (2016) <https://doi.org/10.1002/2015GL066928>
1799
1800
1801
1802 [48] Campitelli, E.: Data for "Evaluating the Importance of Initial Conditions for
1803 Antarctic Sea Ice Seasonal Predictability with a Fully Coupled Forecast Model".
1804 Zenodo (2025). <https://doi.org/10.5281/ZENODO.17479537>
1805
1806
1807
1808
1809
1810
1811
1812
1813
1814
1815
1816
1817
1818
1819
1820
1821
1822
1823
1824
1825
1826
1827
1828
1829
1830
1831
1832
1833
1834
1835
1836
1837
1838
1839
1840